American Mineralogist, Volume 87, pages 25–36, 2002

^{29}Si MAS NMR study of diopside–Ca-Tschermak clinopyroxenes: Detecting both tetrahedral and octahedral Al substitution

ROBERTA L. FLEMMING* AND ROBERT W. LUTH

Department of Earth and Atmospheric Sciences, University of Alberta, Edmonton, Alberta, T6G 2E3, Canada

ABSTRACT

We have studied short-range cation ordering across the diopside ($CaMgSi_2O_6$)-Ca-Tschermak pyroxene ($CaAl_2SiO_6$) (Di-CaTs) solid solution in samples synthesized at 1400 °C and 2 GPa, for 24 hours. Peak positions in ^{29}Si MAS NMR spectra are sensitive to Al substitution, both in the corner-sharing NN tetrahedral sites on the single chain and in one of the three NN octahedral M1 sites. The substitution of Al for Mg on M1 causes the ^{29}Si chemical shift to be shielded by about the same magnitude as the deshielding caused by substitution of Al for Si in NN tetrahedra, causing severe peak overlap among central peaks. Two pairs of the unique local environments have very similar chemical shifts, leaving only four peaks resolved in the spectrum, for which six site assignments have been made.

^{29}Si MAS NMR peak intensities for end-member CaTs are consistent with 70% of the Si in the tetrahedral chain being locally ordered into alternating $^{[4]}$Al-O-Si-O-$^{[4]}$Al linkages, although space group *C*2/*c* would suggest that Si and Al are long-range disordered over the tetrahedral chain. CaTs clearly violates Löwenstein's (1954) Al-O-Al avoidance principle, with 0.175 Al-O-Al linkages per formula unit (based on six O atoms per formula unit), as calculated from observed ^{29}Si MAS NMR peak intensities. For intermediate members of the solid solution, site populations have been modeled using a random distribution model (RD), an Al-O-Al avoidance model (AA) and a modified AA model which couples the cation distribution between the tetrahedral and octahedral sites (AAOC). The RD model fits the ^{29}Si MAS NMR peak intensities poorly. The AA and AAOC models fit the ^{29}Si NMR data well to at least 75% CaTs, suggesting that diopside-rich Di-CaTs clinopyroxenes obey Löwenstein's Al-O-Al avoidance principle. For compositions >75% CaTs, observed cation distributions deviate considerably from that predicted by Al-O-Al avoidance, indicating formation of Al-O-Al linkages. The AAOC model yields an improved fit to the observed ^{29}Si MAS NMR intensities, particularly near $Di_{50}CaTs_{50}$, implying the presence of $^{[4]}$Si-O-$^{[6]}$Mg and $^{[4]}$Al-O-$^{[6]}$Al couples. This suggests the presence of short-range ordering on both tetrahedral and octahedral sites in Di-CaTs pyroxenes.

The high sensitivity to octahedral Al substitution observed in these chain silicates is not observed by ^{29}Si MAS NMR of more-polymerized silicates, such as framework and sheet structures. Thus, ^{29}Si MAS NMR of pyroxenes has potential to reveal tetrahedral-octahedral cation coupling and octahedral cation ordering information, which is potentially important for geothermobarometry of aluminous pyroxenes.

INTRODUCTION

Pyroxenes are major constituents of the Earth's crust and upper mantle to depths of 400 km. They occur in a wide variety of geological settings, both igneous and metamorphic. Their wide stability range and chemical variability make them potentially important indicators of the temperature and pressure conditions of formation. Aluminum-bearing pyroxene can be used to calibrate geothermometers and geobarometers. The presence of aluminous components, such as jadeite ($NaAlSi_2O_6$), Ca-Eskola ($Ca_{0.5}\square_{0.5}AlSi_2O_6$), and Ca-, Mg-, Fe-, Cr-, and Ti-Tschermak pyroxenes ($CaAl_2SiO_6$, $MgAl_2SiO_6$, $FeAl_2SiO_6$, $CaCrAlSiO_6$, $CaTiAl_2O_6$, respectively), is generally correlated with elevated pressures of formation. Tschermak pyroxenes are useful in numerous geobarometers involving both orthopyroxenes (e.g., Carswell 1991; Taylor 1998) and clinopyroxenes (e.g., Putirka et al. 1996; Nimis and Ulmer 1998; Yoshino et al. 1998; Nimis 1995, 1999). A complication that arises in attempting to calibrate or apply these geobarometers is the potential for cation ordering to displace reactions. Configurational entropy and enthalpy accompanying cation disorder in aluminous pyroxenes influences their stability and displaces *P-T* equilibria. Therefore, determination of the cat-

* Present address is Department of Earth Sciences, University of Western Ontario, London, Ontario, N6A 5B7 E-mail: rflemmin@uwo.ca

ion distribution in pyroxenes is essential in order to evaluate the effect on the accuracy of related thermobarometers. To date, however, the extent of Si-Al disorder at the tetrahedral site and X-Al disorder at the octahedral site (where X = Mg, Fe, Ti) is not known.

There is a discrepancy regarding the Si-Al distribution in Ca-Tschermak clinopyroxene (CaTs, $CaAl_2SiO_6$). Crystal-structure determination from X-ray diffraction data (Okamura et al. 1974) has revealed that CaTs has space group *C*2/*c*, consistent with complete disorder at the tetrahedral sites. However, Si and Al cannot be distinguished by X-ray methods due to their similar X-ray scattering behavior. Wood (1976) interpreted activity-composition relations to suggest short-range ordering of tetrahedral Si-Al. He further suggested it could be coupled to octahedral Al distribution. Hays (1966) and Gasparik (1981) determined two different positions in *P-T* space for the equilibrium reaction: $3\ CaAl_2SiO_6 = Ca_3Al_2Si_3O_{12} + 2\ Al_2O_3$. These conflicting results have prevented determination of a definitive zero point entropy (Haselton et al. 1984). Wood and Holloway (1984) suggested that the inconsistencies between these studies could be reconciled if the two sets of pyroxenes had different degrees of Si-Al cation ordering, and hence different configurational entropies. This interpretation suggests that the pyroxenes in Hays (1966) study were disordered, whereas the pyroxenes in Gasparik's (1981) study contained short-range order. Thus, knowledge of the degree of Si-Al ordering in aluminous pyroxenes is essential to evaluating thermodynamic data within the CMAS (CaO-MgO-Al_2O_3-SiO_2) system, but this information is difficult to obtain.

^{29}Si MAS NMR is ideal for examining tetrahedral Si-Al disorder in aluminosilicates. Since the pioneering work of Lippmaa et al. (1980), ^{29}Si MAS NMR has been used to quantify Si-Al disorder in aluminosilicate minerals. Recent examples include framework silicates (e.g., Phillips et al. 1997, 2000; Kato and Hattori 1998; Putnis and Angel 1985), sheet silicates (e.g., Circone et al. 1991; Lausen et al. 1999), double chain silicates (e.g., Welch et al. 1998; Sherriff et al. 1999), and ring silicates (e.g., Armbruster 1999). This technique has not yet been applied systematically to single-chain silicates, such as the pyroxenes.

^{29}Si MAS NMR can establish the local distribution of Al and Si nearest neighbors (NN) around Si, but determining the overall configuration of cations in the mineral requires additional assumptions. One common assumption is Löwenstein's principle of Al-O-Al avoidance (Löwenstein 1954), which asserts that the Al-O-Si linkage is energetically more favorable than the combination of Si-O-Si and Al-O-Al linkages. This assumption has commonly been a starting point for interpretation of Si NMR spectra (e.g., Kato and Hattori 1998; Welch et al. 1998; Lausen et al. 1999). If Löwenstein's principle is obeyed, tetrahedral Si/Al site population ratios can be calculated directly from ^{29}Si MAS NMR spectra. Conversely, if the tetrahedral Si/Al ratio of a mineral is known, the number of Al-O-Al linkages can be calculated as the difference between the Si/Al ratio expected for complete Al-O-Al avoidance and that observed in the ^{29}Si MAS NMR spectrum (see Kirkpatrick 1988). Although the Al-O-Al avoidance principle has a thermodynamic basis (e.g., Tossell 1993; Myers et al. 1998) it is not strictly obeyed for framework silicates (e.g., Phillips et al. 1992, 2000; Cheng et al. 2000). Al-O-Al avoidance is, however, obeyed in sheet silicates (Sanz and Serratosa 1984; Circone et al. 1991; Vinograd and Putnis 1998). The Al-O-Al avoidance principle has not been tested for aluminous pyroxenes, but energy calculations by Cohen and Burnham (1985) predicted that it would hold. It can be tested for end-member CaTs ($CaAl_2SiO_6$) where $^{[4]}(Si/Al) = 1$.

Compositions across the Di-CaTs solid solution follow the general formula $Ca[Mg_{1-x}Al_x](Si_{1-x/2}Al_{x/2})_2O_6$, where ( ) and [ ] represent the tetrahedral and octahedral sublattices, respectively. Cation substitution is governed by Tschermak's substitution $(Si^{+4}) + [Mg^{+2}] = (Al^{+3}) + [Al^{+3}]$. Clinopyroxenes of intermediate composition are complicated by cation order-disorder occurring simultaneously on both the tetrahedral and octahedral sublattices. These pyroxenes contain single chains of corner-sharing tetrahedra parallel to **c**, occupied by Si or Al. Parallel to the tetrahedral chains are zigzag chains of edge-sharing M1 octahedra occupied by Mg or Al (Cameron and Papike 1981). It has not yet been established whether cation ordering on the tetrahedral and octahedral sites is correlated in Tschermak pyroxenes. The 8-coordinated M2 sites also form chains parallel to **c**. This site remains solely occupied by Ca across the solid solution and is not involved in cation disorder in Di-CaTs pyroxenes.

Herein we present a systematic ^{29}Si MAS NMR investigation of aluminous pyroxenes, with data from six compositions across the Diopside-CaTs solid solution ($CaMgSi_2O_6$-$CaAl_2SiO_6$). For end-member CaTs, we calculate the number of Al-O-Al linkages from the observed ^{29}Si MAS NMR spectrum. ^{29}Si MAS NMR spectra of intermediate compositions suffer from severe peak overlap, resulting from disorder on both octahedral and tetrahedral sublattices. To extract intensity information from the overlapping peaks, we have modelled the cation distribution across the solid solution using a random distribution model (RD), an Al-O-Al avoidance model (AA), and a modified AA model that imposes tetrahedral-octahedral cation coupling (AAOC).

Experimental methods

Sample synthesis and characterization

Compositions along the Diopside-Ca-Tschermak (Di-CaTs) solid solution, including Di_{100}, $Di_{95}CaTs_{05}$, $Di_{75}CaTs_{25}$, $Di_{50}CaTs_{50}$, $Di_{25}CaTs_{75}$, and $CaTs_{100}$, were crystallized from anhydrous glasses at 2 GPa and 1400 °C for 24 hours. Starting glasses were prepared from stoichiometric mixtures of MgO (AESAR 99.99%), Al_2O_3 (AESAR 99.99%) and SiO_2 (AESAR 99.5%), each dried at 1000 °C overnight, and $CaCO_3$ (AESAR 99.97%), dried at 400 °C for 5 hours. Starting mixtures were hand ground for one hour in an agate mortar and pestle and were placed in platinum crucibles. Crucibles were heated at 1000 °C for 2 hours, then 1200 °C for 2 hours to decarbonate, and then fused at 1600 °C. Samples were fused at 1600 °C for three hours and quenched by placing the crucible in cold water, to produce glass. Samples were then hand ground in an agate mortar and pestle for one hour, fused at 1600 °C for an additional three hours, and then quenched and ground to a powder.

Glass samples were loaded into 5 mm diameter Pt-capsules, dried at 120 °C for 12–24 hours and welded closed. The capsules were run vertically, in 19 mm diameter talc-pyrex furnace assemblies of the Kushiro (1976) design. A pressure correction of –13% was applied based on calibration of the reaction Grt + Qtz = An + Wo. Temperatures were monitored using $W_{95}Re_{05}$-$W_{74}Re_{26}$ thermocouples in 99.99% alumina sleeves, with no pressure correction applied to thermocouple electromotive force.

Samples were characterized by electron probe microanalysis (EPMA) and X-ray powder diffraction (XRD). The JEOL 8900 electron probe was operated in WDS mode, using a beam current of 20 nA and an acceleration voltage of 15 kV. Natural diopside (Mg, Si), kyanite (Al) and wollastonite (Ca) were used as calibration standards. Data were corrected using the ZAF correction method provided by JEOL. Sample chemistry is summarized in Table 1. Samples are stoichiometric within error. CaTs (sample RM010K) appears slightly Al-depleted, but this value is more likely to be an artifact of the analysis. The measured wt% Al is only 0.6% lower than expected value of 46.74% (a relative difference of only 1.3%), but this low value for Al was exaggerated by an unrealistically high value for Ca. The Ca value was only 0.49 wt% above its expected value of 25.71 wt% (or 1.9%) but this yields 1.02 Ca pfu, whereas the structure can only accommodate 1.00 Ca pfu. Reducing the wt% Ca to correspond to 1.00 Ca pfu and recalculating the chemical formula yields 1.985 Al pfu, which is essentially stoichiometric within the standard deviation of the analysis. Thus, we believe CaTs to be stoichiometric. If it were Al-depleted, we assume any vacancies would occur at M1, such that $^{[4]}$Al/Si = 1.

Examination by back-scattered electron imaging on the electron microprobe revealed that some samples contained minor SiO_2, Al_2O_3 or anorthite as extra phases. Both SiO_2 and anorthite were not detected by XRD, indicating that they were present in amounts less than 1–3%. The presence of SiO_2 would not influence peak intensities in the ^{29}Si NMR spectrum of Di-CaTs because its chemical shift is well removed (–107 to –114 ppm depending on crystal form) (Sherriff et al. 1991). The presence of significant anorthite would interfere with the ^{29}Si NMR spectra of Di-CaTs pyroxenes, because it has peaks at –82.7, –84.7 and –89.3 ppm (Sherriff et al. 1991). However, the amount of anorthite found in sample RM010K is estimated to be small (<3%). Corundum was detected by XRD, indicating >1–2% abundance, but Al_2O_3 is invisible to ^{29}Si MAS NMR.

Crystal-structure information from Rietveld refinement of X-ray powder diffraction data will be presented elsewhere. Structures are consistent with space group *C*2/*c*, which implies long-range disorder of Si-Al on the tetrahedral sublattice.

^{29}Si MAS NMR spectroscopy

^{29}Si MAS NMR spectra were acquired on a Bruker AM-R 300 spectrometer at 59.6 MHz (7.05 Tesla) using a Bruker variable frequency CP-MAS probe. Samples were placed in 7 mm rotors (about half filling the rotor), with spinning rates of 4–5 kHz. Chemical shifts were measured relative to synthetic forsterite (–61.8 ppm), which was referenced to TMS. A relaxation delay of 300 s was used together with a pulse angle of ~30° or 1.5 ms, relative to the spectrometer π/2 pulse width of 5ms (power level 4 DB). Preliminary experiments at variable relaxation delays revealed 300 s to be adequate time to allow samples to recover essentially full magnetization. Typically ~1100 scans were added to produce each spectrum [excepting diopside (580 scans) and CaTs (800 scans)]. Spectra were acquired with 16 K data points and a spectral width of ~24,000 Hz, and Fourier transformed with 20 Hz line broadening. Spectral peaks were fitted using the program NUTS (Acorn NMR Inc., Fremont, CA) to give chemical shift, peak width, and relative intensity information.

Results

^{29}Si MAS NMR spectra

^{29}Si MAS NMR spectra for the six samples across the diopside-CaTs solid solution are shown in Figure 1. Variations in chemical shift, peak intensity and peak width across the solid solution are summarized in Table 2, and are consistent with previous data (Cohen 1985; Warren et al. 2001). The ^{29}Si MAS

Table 1. Chemical analyses for Di-CaTs pyroxenes and extra phases from EPMA

Sample	RM011B		RM012A		RM009D		RM006E		RM008C		RM010K	
Composition	Di_{100}		$Di_{95}CaTs_{05}$		$Di_{75}CaTs_{25}$		$Di_{50}CaTs_{50}$		$Di_{25}CaTs_{75}$		$CaTs_{100}$	
wt% oxides												
MgO	18.30	(0.19)*	17.60	(0.34)*	13.92	(0.52)*	9.27	(0.39)*	4.60	(0.23)*	0.01	(0.00)*
CaO	25.88	(0.23)	25.91	(0.27)	25.91	(0.37)	25.75	(0.51)	25.31	(0.58)	26.20	(0.13)
Al_2O_3	0.06	(0.01)	2.41	(0.19)	11.63	(0.21)	23.57	(0.47)	35.08	(0.33)	46.14	(0.35)
SiO_2	54.98	(0.17)	53.84	(0.28)	48.53	(0.25)	41.39	(0.33)	34.33	(0.27)	27.70	(0.27)
Total	99.22		99.76		99.99		99.98		99.32		100.05	
Cations per formula unit (6 O atoms)												
Mg	0.992	(0.009)	0.948	(0.017)	0.749	(0.026)	0.500	(0.020)	0.250	(0.012)	0.000	(0.000)
Ca	1.008	(0.007)	1.003	(0.010)	1.003	(0.016)	0.998	(0.021)	0.989	(0.021)	1.019	(0.006)
Al	0.002	(0.001)	0.103	(0.008)	0.495	(0.009)	1.005	(0.019)	1.509	(0.014)	1.975	(0.013)
Si	1.998	(0.003)	1.946	(0.005)	1.753	(0.007)	1.497	(0.013)	1.252	(0.011)	1.006	(0.009)
Total†	4.000		4.000		4.000		4.000		4.000		4.000	
No. analyses	23		22		24		11		22		10	
Extra phases	SiO_2		–		–		–		–		Crn + An	

Notes: Chemical formulae follow general formula $CaMg_{1-x}Al_{2x}Si_{2-x}O_6$, where x = mole fraction CaTs component. EPMA = Electron probe microanalysis, Crn = corundum, An = anorthite.

* Number in parentheses is standard deviation over total number of analyses.

† Totals are normalized to 4.000 cations.

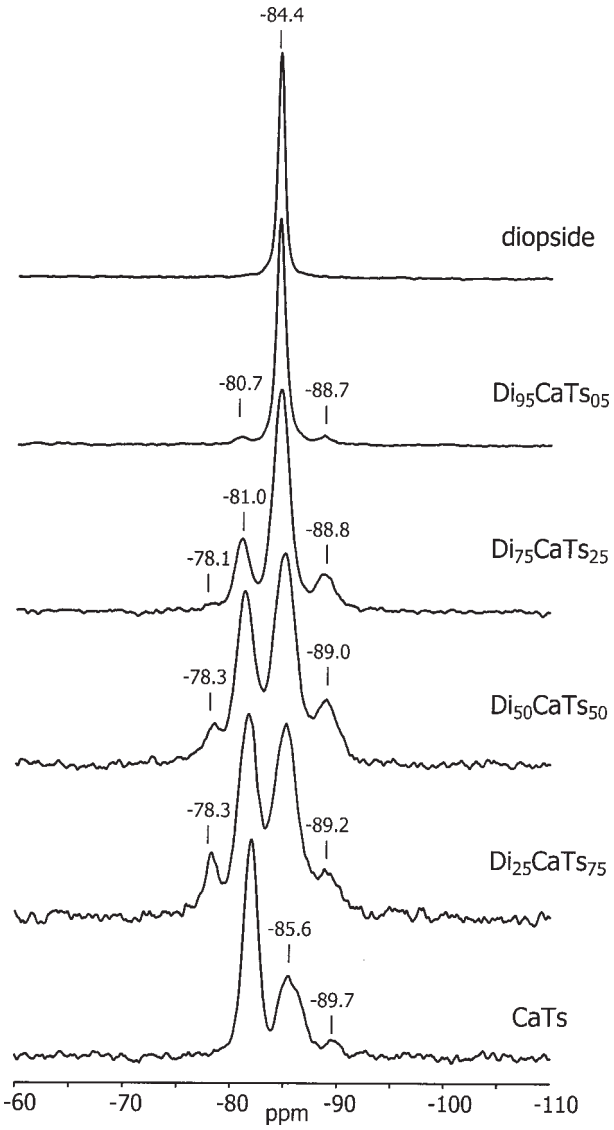

FIGURE 1. ^{29}Si MAS NMR spectra for six compositions along the diopside-CaTs solid solution. Numbers refer to chemical shifts in ppm.

NMR spectrum of diopside (Fig. 1, top spectrum) exhibits a narrow (45 Hz) single peak at –84.4 ppm, consistent with previous results (e.g., Kirkpatrick et al. 1985). The narrow peak results from a single, ordered environment around Si. The spectrum of end-member CaTs (Fig 1. bottom spectrum) exhibits three broad peaks, consistent with the results of Cohen (1985). Multiple peaks are the result of Si-Al disorder over the tetrahedral sites (as octahedral sites in CaTs contain only Al). Spectra of intermediate compositions exhibit multiple peaks, resulting from cation disorder on both the tetrahedral and octahedral sublattices. Four peaks are easily resolved in the ^{29}Si MAS NMR spectra of $Di_{75}CaTs_{25}$, $Di_{50}CaTs_{50}$ and $Di_{25}CaTs_{75}$ (see Fig 1). Our ^{29}Si MAS NMR spectrum of $Di_{50}CaTs_{50}$ is consistent with that of Warren et al. (2001) but differs from that obtained by Cohen (1985) in which only three peaks were resolved. Cohen's spectra did not have a peak near –78 ppm. This difference may result from the lower signal-to-noise ratio in his spectra, or from a different degree of ordering in his sample. The ^{29}Si MAS NMR spectra from intermediate compositions are complicated by severe peak overlap. The NMR peak assignments are listed in Table 2, and are explained in the next section.

^{29}Si MAS NMR peak widths increase with increasing CaTs component, consistent with increasing cation disorder accompanying addition of Al. For example, the peak near –85 ppm continuously increases in width with addition of Al, from 45 Hz in diopside to 155 Hz in CaTs. The other peaks reach their maximum widths for intermediate members of the solid solution due to cation disorder on both sublattices (see Table 2). Close examination of the four peaks reveals irregular line shapes as well as peak broadening. This indicates that these peaks are not true single peaks, but are chemical shift dispersions, likely resulting from cation substitution at the various M1 sites and/or distant tetrahedral sites such as on adjacent chains.

Also the positions of each of the four peak centroids change slightly but continuously by about –1 ppm to lower frequency with increasing tetrahedral Al/Si ratio in the structure, across the solid solution (see Table 2). This trend has been reported for glasses along the diopside -CaTs join by Kirkpatrick et al. (1986), and for aluminous phlogopites by Circone et al. (1991).

TABLE 2. ^{29}Si MAS NMR chemical shift, peak intensity, and peak width variation across the Di-CaTs solid solution

Sample number	RM011B	RM012A	RM009D	RM006E	RM008C	RM010K
Composition	Di_{100}	$Di_{95}CaTs_{05}$	$Di_{75}CaTs_{25}$	$Di_{50}CaTs_{50}$	$Di_{25}CaTs_{75}$	$CaTs_{100}$
Peak Assignments* (below):			**Chemical shift (d_{obs}) (ppm)**			
Si(2Al)[0Al]	–	–	–78.1	–78.3	–78.3	–
Si(1Al)[0Al] + Si(2Al)[1Al]	–	–80.7	–81.0	–81.3	–81.6	–81.9
Si(0Al)[0Al] + Si(1Al)[1Al]	–84.4	–84.5	–84.6	–85.0	–85.2	–85.6
Si(0Al)[1Al]	–	–88.7	–88.8	–89.0	–89.2	–89.7
			Peak intensity (I) (%)			
Si(2Al)[0Al]	–	–	2	6	11	–
Si(1Al)[0Al] + Si(2Al)[1Al]	–	2	21	37	41	70
Si(0Al)[0Al] + Si(1Al)[1Al]	100	95	67	46	41	25
Si(0Al)[1Al]	–	3	10	11	7	5
			Peak width (FWHM) (Hz)			
Si(2Al)[0Al]	–	–	71	86	70	–
Si(1Al)[0Al] + Si(2Al)[1Al]	–	71	95	117	115	94
Si(0Al)[0Al] + Si(1Al)[1Al]	45	59	106	143	147	154
Si(0Al)[1Al]	–	79	111	137	120	81

* Peak assignments follow general formula Si(nAl)[mAl] (n = 0, 1, 2; m = 0, 1).

^{29}Si NMR site assignments in Di-CaTs clinopyroxenes

The single peak at –84.4 ppm in the ^{29}Si MAS NMR spectrum of diopside (Fig 1, top spectrum) can be conventionally assigned to Si(0Al) [where (nAl) is the number of NN tetrahedral Al corner-sharing with Si], as there is no Al in diopside. For each Si in diopside, the two corner-sharing NN tetrahedral sites are occupied by Si, while the three NN octahedral M1 sites are occupied by Mg.

The spectrum of end-member CaTs (Fig. 1, bottom spectrum) exhibits three peaks, at –89.7, –85.6, and –81.9 ppm. According to the well-established deshielding of the ^{29}Si nucleus (peak movement to higher frequency; more positive ppm value) with substitution of Al for Si at a corner-sharing NN tetrahedral site (Fyfe 1983; Engelhardt and Michel 1987; Kirkpatrick 1988), the three peaks in end-member CaTs can be assigned as Si(0Al), Si(1Al) and Si(2Al), respectively. Successive substitution of Al into corner-sharing NN tetrahedral sites causes the chemical shift to step incrementally to higher frequencies, by about +4 ppm in this case.

However, comparison of the chemical shift for Si(0Al) in diopside (–84.4 ppm) and CaTs (–89.7 ppm) shows them to differ by –5.3 ppm. Accounting for the peak centroid shift of about –1 ppm across the solid solution (as discussed above), there remains an approximately –4 ppm displacement of the Si(0Al) peak, toward greater shielding of the ^{29}Si nucleus in CaTs (peak movement to lower frequency; more negative ppm value). We postulate that the increased shielding in CaTs results from substitution of Al at the octahedral site in CaTs for Mg at the octahedral site in diopside. Increased shielding with substitution of Al for Mg at the octahedral site is consistent with previous NMR studies of orthosilicates and chain silicates, where the effectiveness of octahedral shielding by Al has been shown to increase with decreasing polymerization of the silicate (Kirkpatrick et al. 1985).

Thus, ^{29}Si NMR spectra of aluminous pyroxenes exhibit sensitivity to Al substitution on both the tetrahedral and octahedral sites. To accommodate this effect, we have modified the conventional nomenclature to reflect the presence or absence of Al in the NN octahedral M1 site bonded to Si, by adding the symbol [1Al] or [0Al], respectively (where square brackets indicate the octahedral environment). Thus, the diopside peak at –84.4 ppm, is assigned as Si(0Al)[0Al], to indicate the absence of Al in the NN octahedral M1 sites, while the three peaks in CaTs at –89.7, –85.6, and –81.9 ppm, are assigned as Si(0Al)[1Al], Si(1Al)[1Al] and Si(2Al)[1Al], respectively, to indicate the presence of Al in the NN octahedral M1 sites bonded to Si. The site assignments for CaTs are indicated on the ^{29}Si MAS NMR spectrum of CaTs in Figure 2. We denote chemical shifts in aluminous pyroxenes using the general formula Si(nAl)[mAl] (n = 0, 1, 2; m = 0, 1), where ( ) and [ ] indicate neighboring tetrahedral and octahedral Al, respectively.

Using this assignment, we have been able to systematically interpret the spectra of intermediate Di-CaTs compositions, when conventional site assignments [i.e., Si(0Al), Si(1Al), and Si(2Al)] clearly cannot explain the appearance of four peaks in the NMR spectra of intermediate members of the solid solution. To illustrate site assignments for intermediate members of the solid solution, we now describe the ^{29}Si MAS NMR spectrum of $Di_{50}CaTs_{50}$ shown in Figure 3. The peak at –85.0 ppm in Figure 3 can be assigned as Si(0Al)[0Al] because it is in approximately the same position as the single peak in Al-free diopside (–84.4 ppm). Similarly the peaks at –81.6 and –78.3 ppm, are assigned to Si(1Al)[0Al] and Si(2Al)[0Al] respectively, as a result of systematic deshielding (by about +4 ppm/Al) by Al substitution at the two NN tetrahedral sites sharing corners with Si on the single chain, while Mg is assumed to occupy the octahedral site.

The fourth peak, at –89.0 ppm in the spectra of intermediate Di-CaTs pyroxenes, which is more shielded than Si(0Al)[0Al], is assigned as Si(0Al)[1Al] because it is in the same position as the Si(0Al)[1Al] peak in end-member CaTs. In our interpretation, this peak results from substitution of Al for Mg at one of the three M1 octahedral sites bonded to Si. This increases the shielding around Si, producing a shift to lower frequency by approximately –4 ppm. However, the –4 ppm shift

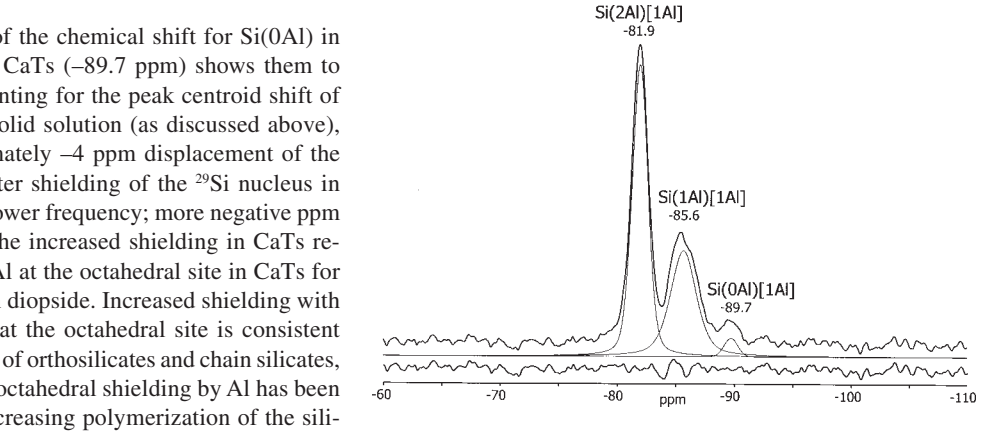

FIGURE 2. ^{29}Si MAS NMR spectrum of end-member CaTs, showing observed spectrum (upper trace), simulated lines (thin middle traces) and the difference spectrum (lower trace) (derived from observed peak intensity minus simulated line intensity). Numbers refer to chemical shifts in ppm. Peak assignments are indicated on the diagram.

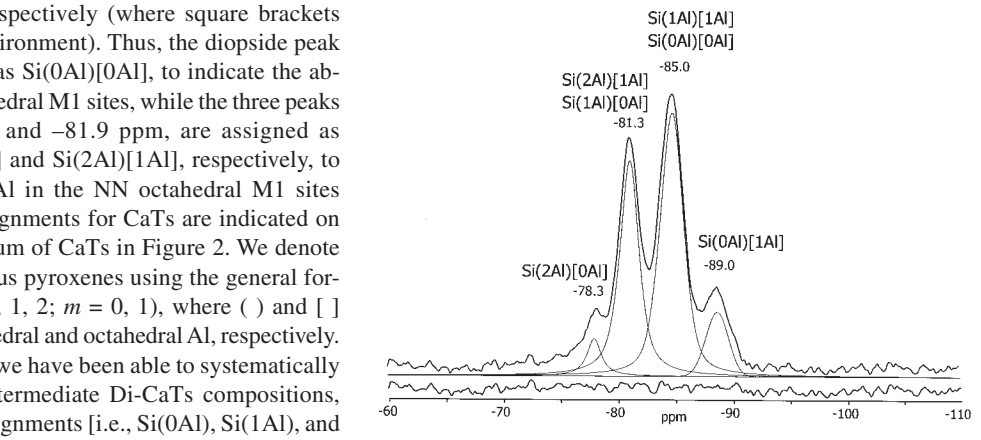

FIGURE 3. ^{29}Si MAS NMR spectrum of $Di_{50}CaTs_{50}$, showing observed spectrum (upper trace), simulated lines (thin middle traces) and the difference spectrum (lower trace). Numbers refer to chemical shifts in ppm. Peak assignments are indicated on the diagram.

upon substitution of Al for Mg at the M1 site must be applied to all three of the original Si(nAl)[0Al] sites, thus producing three additional lower-frequency sites. Thus, each of the three original Si environments, i.e., Si(0Al)[0Al], Si(1Al)[0Al], and Si(2Al)[0Al], containing no NN octahedral Al, are shifted by about –4 ppm upon substitution of Al for Mg at the octahedral M1 site, to produce three additional sites, which are assigned as Si(0Al)[1Al], Si(1Al)[1Al], and Si(2Al)[1Al]. Thus, there are a total of six site assignments for the four peaks in the NMR spectra of intermediate members of the Di-CaTs solid solution, as indicated in Figure 3. Each of the two central peaks contains two Si environments with almost identical chemical shifts, resulting in two pairs of severely overlapped peaks. The peak at –85.0 ppm contains Si(0Al)[0Al] + Si(1Al)[1Al], and the peak at –81.3 ppm contains Si(1Al)[0Al] + Si(2Al)[1Al]. Serendipitously, in Di-CaTs clinopyroxenes, the effects of octahedral and tetrahedral Al substitution are essentially the same in magnitude but opposite in sign. Tetrahedral Al substitution is essentially "cancelled out" by octahedral Al substitution.

Discussion

Sensitivity to Al substitution at the octahedral site

Comparison of the ^{29}Si MAS NMR spectra (Fig. 1) shows that continuous substitution of Al into octahedral sites does not have an additive effect on chemical shift as with tetrahedral Al substitution (i.e., there is no stepwise shift to lower frequency with increasing Al substitution into M1). This begs the question, "How sensitive is ^{29}Si MAS NMR to Al substitution at the octahedral sites?" Because the three M1 sites around Si are not symmetrically arranged, is Si sensitive to Al at only the closest M1 site or at all three NN M1 sites [at distances of 3.172, 3.257 and 3.415 Å, in $Di_{50}CaTs_{50}$, for example (distances from Benna et al. 1988)]. These questions can be answered by considering the ^{29}Si MAS NMR spectrum of $Di_{95}CaTs_{05}$ (Fig. 1, second spectrum from top). The large central peak (–84.4 ppm, I = 95%) can be assigned as Si(0Al)[0Al], being consistent with 95% diopside component in the sample. The remaining 5% of the sample contains Al due to the CaTs component, where Tschermak's substitution ensures that Al enters both octahedral and tetrahedral sites. In this dilute system it is statistically unlikely that Al would occupy both a tetrahedral and an octahedral site around the same Si atom, suggesting that the two small peaks, at higher and lower frequencies than the diopside peak, represent Si(1Al)[0Al] (–80.7 ppm, I = 2%) and Si(0Al)[1Al] (–88.7 ppm, I = 3%), respectively. Structurally, each M1 site is surrounded by six NN tetrahedral Si atoms, while each tetrahedral site (T) has two corner sharing NN tetrahedral Si atoms. From the structural formula for $Di_{95}CaTs_{05}$, $Ca[Mg_{0.95}Al_{0.05}](Si_{0.975}Al_{0.025})_2O_6$, and considering that each Si(0Al)[0Al] site is enumerated twice by ^{29}Si NMR, and normalizing Si(1Al)[0Al] and Si(0Al)[1Al] intensities by one half, the ^{29}Si MAS NMR spectrum would be expected to show 15% intensity for Si(0Al)[1Al] if all six Si surrounding M1 were sensitive to Al in M1. However, if only two of the six Si atoms were sensitive to Al substitution in M1, the ^{29}Si MAS NMR spectrum would be expected to show 5% Si(0Al)[1Al]. This value is closer to the observed intensity of 3% for Si(0Al)[1Al] in the ^{29}Si MAS NMR spectrum, suggesting that only 1/3 of the Si atoms surrounding M1 are sensitive to Al substitution, or equivalently, that Si is sensitive to only one in three NN octahedral M1 sites. We therefore make the assumption that the –4 ppm peak shift to low frequency observed in the ^{29}Si MAS NMR spectrum is due to substitution of Mg for Al only at one specific M1 site. We suggest that the "sensitive" M1 site is the M1 bonded to Si through O2, as O2 is underbonded relative to O1 (Okamura et al. 1974) (O2 is 3-coordinated while O1 is 4-coordinated). Crystallographically, this M1 site is closest to Si (T-M1 = 3.172 Å) and the T-O2 and M1-O2 bond distances are shorter than the T-O1 and M1-O1 bond distances, respectively (e.g., $Di_{50}CaTs_{50}$: T-O2 = 1.623 Å versus T-O1 = 1.646 Å; M1-O2 = 1.969 Å vs. M1-O1 = 1.999 and 2.066 Å; Benna et al. 1988).

Because it appears that Al substitution at only one of the three NN octahedral M1 sites around Si affects the ^{29}Si MAS NMR chemical shift, we have treated M1 as a single site in our peak intensity models, subsequently discussed. Small differences in chemical shift, likely induced by substitution at the other M1 sites, may be the cause of increased chemical shift dispersion and peak broadening observed for the four resolved peaks at intermediate compositions (see Table 2).

Site populations in the CaTs spectrum (Al/Si = 1)

Peak assignments for end-member CaTs are straightforward because there is no peak overlap. The octahedral sites are entirely occupied by Al. Thus the number of Al-O-Al linkages in CaTs can be calculated directly from its ^{29}Si MAS NMR spectrum. Figure 2 shows the spectrum of end-member CaTs, together with simulated lines and difference spectrum. Peaks Si(2Al)[1Al], Si(1Al)[1Al], and Si(0Al)[1Al] (–81.9, –85.6, and –89.7 ppm, respectively) have intensities of 70%, 25%, and 5%, respectively. A peak intensity of 70% for Si(2Al)[1Al] implies that 70% of the Si atoms are locally ordered into alternating $^{[4]}$Al-O-Si-O-$^{[4]}$Al tetrahedra. This structure is highly short-range ordered to facilitate Al-O-Al avoidance, but it is not fully ordered as indicated by multiple peaks in the ^{29}Si NMR spectrum. In end-member CaTs, perfect Al-O-Al avoidance is only possible for the fully long-range ordered structure, composed entirely of chains of alternating $^{[4]}$Al-O-Si-O-$^{[4]}$Al-O-Si tetrahedra.

The relationship between ^{29}Si NMR peak intensities, disorder, and number of Al-O-Al linkages in CaTs can be understood visually, using the schematic CaTs clinopyroxene in Figure 4. The tetrahedral chain in Figure 4a shows CaTs which is fully ordered, with alternating Al and Si tetrahedra, showing only Si(2Al) sites. Switching a pair of Al and Si atoms along the chain produces two Si sites having only one tetrahedral Al NN [denoted Si(1Al)] and one Al-O-Al linkage, as in Figure 4b. Switching a pair adjacent to the first pair will produce an Si site having no tetrahedral Al NN [denoted Si(0Al)], and an additional Al-O-Al linkage, as seen in Figure 4c. Clearly, any disorder on the tetrahedral chain in CaTs will produce Al-O-Al linkages, which can be enumerated from the intensities of the Si(0Al) and Si(1Al) peaks in the ^{29}Si MAS NMR spectrum.

For compounds with $^{[4]}$(Si/Al) = 1, such as end-member CaTs, the number of Al-O-Al linkages can be calculated from

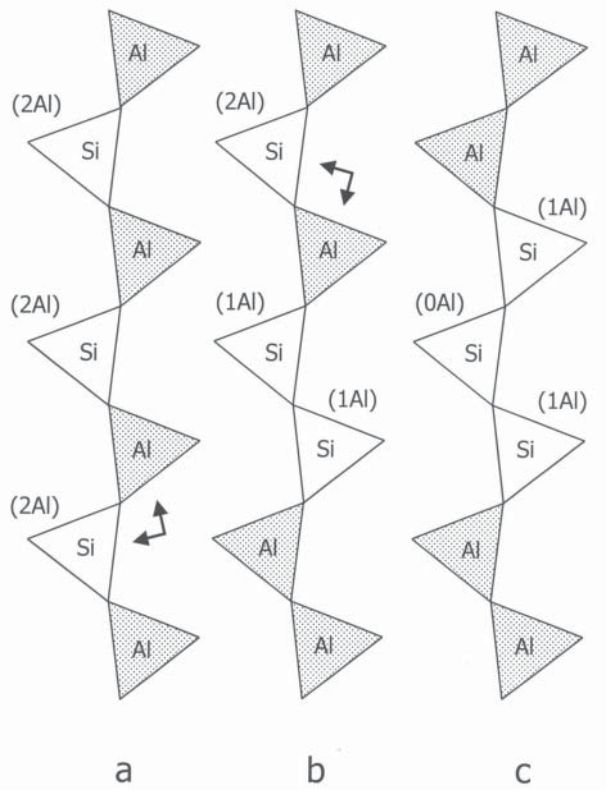

FIGURE 4. Schematic drawing of tetrahedral chain in CaTs pyroxene, showing the relationship between ^{29}Si NMR peak intensities and the number of Al-O-Al linkages. (**a**) Completely ordered tetrahedral chain with alternating Al and Si tetrahedra [all Si are Si(2Al)]. (**b**) Chain after switching one pair of Al-Si tetrahedra (as indicated by arrow) to produce two Si-O-Si-O-Al linkages [Si(1Al)] and one Al-O-Al linkage. (**c**) Chain after switching two pairs of Al-Si tetrahedra to produce one Si-O-Si-O-Si linkage [Si(0Al)], two Si-O-Si-O-Al linkages [Si(1Al)], and two Al-O-Al linkages.

the following relationship developed by Phillips et al. (1997) (adapted for pyroxenes): N(Al-O-Al) = N (Si-O-Si) = $1/2\sum(2 - n)\cdot I(Si(nAl))$, where N is the number of Al-O-Al linkages. By this relationship, our CaTs sample, having 70% Si(0Al)[1Al], 25% Si(1Al)[1Al], and 5% Si(0Al)[1Al], yields 0.175 Al-O-Al linkages per formula unit (pfu) (based on six O atoms). This is equivalent to 35% disorder in the structure relative to 0.50 Al-O-Al linkages in the random case. This compares well with 0.185 Al-O-Al linkages pfu in Cohen's (1985) sample (or 37% disordered), as calculated from the ^{29}Si MAS NMR intensity data of Cohen (1985). ^{29}Si MAS NMR intensity data was not given by Warren et al. (2001).

Our measured value of 0.175 Al-O-Al linkages pfu in pyroxene is comparable to 0.19 Al-O-Al linkages pfu observed in anorthite (Phillips et al. 1992). However, Sherriff et al. (1998) measured as many as 0.60 Al-O-Al linkages pfu in natural scapolites of intermediate composition. Non-equilibrium cation distributions can be a problem in synthetic samples. Phillips et al. (2000) observed 0.55 Al-O-Al linkages pfu for unequilibrated β-eucryptite, after annealing only one hour at 900 °C, which decreased to 0.05 Al-0-Al linkages pfu after 70.5 hours of annealing. Similarly, our samples, although heated for 24 hours at 1400 °C and 2 GPa, may not have achieved an equilibrium cation distribution.

Modeling of Al distribution for intermediate members of the solid solution

For intermediate members of the diopside-CaTs solid solution, quantitative interpretation of ^{29}Si MAS NMR peak intensities is complicated by peak overlap. To extract site population information from the two pairs of completely overlapping central peaks, we have applied three simple statistical models. These are the random distribution model, and two variations of the Al-O-Al avoidance model as modified from Herrero et al. (1985) for mica. It was necessary to modify Herrero et al.'s (1985) Al-O-Al avoidance model to use it for pyroxenes, as well as to investigate the suspected association between cation distributions on the tetrahedral and octahedral sublattices. In each of the three models, a three-site assumption was used. We considered Si to be surrounded by three cation sites only: two corner sharing NN tetrahedral sites on the single chain, and one NN octahedral M1 site. Although there are three M1 sites around each Si atom, ^{29}Si MAS NMR peak intensity appears to be most strongly affected by Al substitution at only one M1 site. We have suggested above that the "sensitive" site would likely be M1 sharing the underbonded O2 with Si. The three models for cation distribution are discussed.

Random distribution model

Cation occupancies at two tetrahedral sites and one octahedral M1 site around Si (three-site assumption, as described above) were calculated according to their statistical probability assuming that there is no restriction on the occupancy of the neighboring tetrahedra or octahedra. For compositions along the diopside–CaTs solid solution, site probabilities are related to mole fraction of each species according to general formula $Ca[Mg_{1-x}Al_x](Si_{1-x/2}Al_{x/2})_2O_6$, where ( ) and [ ] represent the tetrahedral and octahedral sublattices, respectively. Site probabilities were calculated as a binomial series based on fractional contents at the three sites, as outlined in Appendix 1.1. The configuration of neighboring tetrahedra and octahedra determines both the position and site assignment of the peak, while the population of each configuration determines its calculated intensity contribution to the ^{29}Si MAS NMR spectrum.

Peak intensities calculated using the RD model are compared to observed ^{29}Si MAS NMR peak intensities across the Di-CaTs solid solution in Figure 5. The random model is a reasonable fit to the data only for dilute Al content, <25% CaTs component, consistent with the suggestion of Cohen (1986a). At higher concentrations of CaTs, the RD model is clearly a poor fit to the experimental NMR data, illustrating that the cation distribution in Di-CaTs pyroxenes is non-random, despite the long-range disorder implied by space group *C*2/*c*. A non-random cation distribution in Tschermak pyroxenes has been predicted from thermodynamic calculations (e.g., Ganguly and Ghose 1979; Cohen and Burnham 1985) and is well known in other aluminosilicates (e.g., Herrero et al. 1985). The Al-O-Al avoidance models outlined below fit the ^{29}Si MAS NMR data significantly better than the RD model.

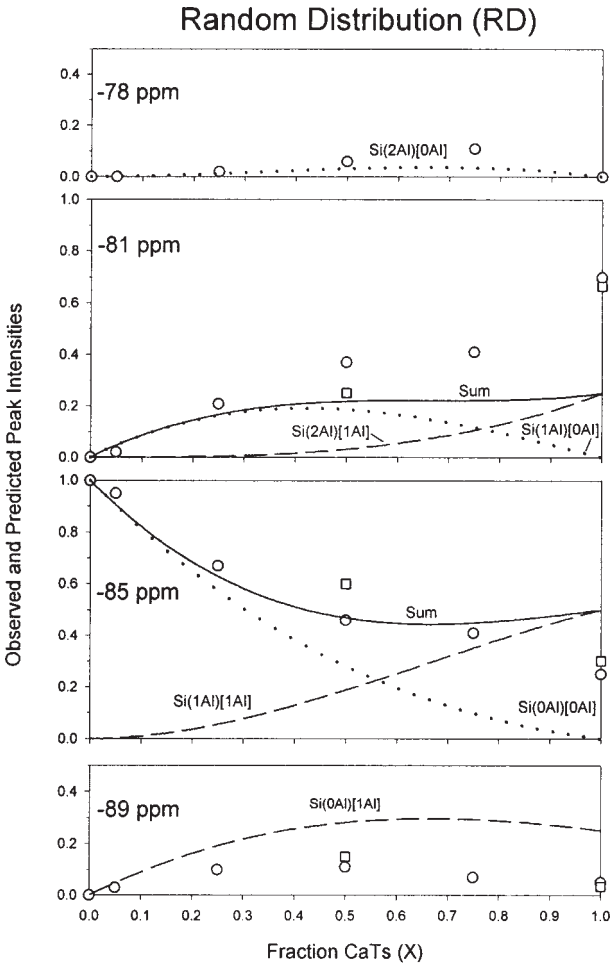

FIGURE 5. Comparison of observed ^{29}Si MAS NMR peak intensities across the diopside-CaTs solid solution with site populations predicted using the Random Distribution model (RD). The four NMR peaks, near –78 ppm, –81 ppm, –85 ppm, –89 ppm, are shown in **upper** to **lower** boxes, respectively. Circles indicate observed ^{29}Si MAS NMR peak intensities from this study. Squares indicate observed ^{29}Si MAS NMR peak intensities from Cohen (1985). Lines indicate predicted site populations, where dotted lines indicate the absence of octahedral Al [i.e., Si(nAl)[0Al]], dashed lines indicate the presence of octahedral Al [i.e., Si(nAl)[1Al]], and solid lines indicate the total calculated intensity for peaks where overlap occurs (sum of dotted and dashed lines). For each peak position, the total calculated intensity should approximate the observed NMR intensity (circles) for closest fit. Note that observed and calculated intensities are each normalized such that the sum of intensities over the four peaks equals one, for any composition. Site assignments for predicted site populations (i.e., dashed and dotted lines) are labeled on the figure. The RD model is a poor fit to the observed NMR data.

Al-O-Al avoidance model

This model applies the Al-O-Al avoidance principle first postulated by Löwenstein (1954). This principle assumes that there is a non-random distribution of Si and Al over the tetrahedral sites, where Al-O-Al linkages are avoided due to electrostatic energy considerations (e.g., Cohen and Burnham 1985). Assuming complete Al-O-Al avoidance, there are only two possible bonding associations: Si-O-Al and Si-O-Si. As outlined in Appendix 1.2, the probability of Al occurring beside Si is related to the tetrahedral Al/Si ratio for the pyroxene. The normalized probabilities for Si-O-Al and Si-O-Si are $P_{Si\text{-}O\text{-}Al} = (Al/Si)$ and $P_{Si\text{-}O\text{-}Si} = (1 - Al/Si)$, respectively. It follows that $P_{Al\text{-}O\text{-}Si\text{-}O\text{-}Al} = (Al/Si)^2$, $P_{Si\text{-}O\text{-}Si\text{-}O\text{-}Si} = (1 - Al/Si)^2$ and $P_{Si\text{-}O\text{-}Si\text{-}O\text{-}Al} = 2(Al/Si)(1 - Al/Si)$. In this model, it has been assumed that the octahedral distribution of Mg and Al is random (i.e., $P^{M1}_{Mg} = 1 - x$ and $P^{M1}_{Al} = x$). This assumption is consistent with *C*2/*c* pyroxenes exhibiting no detectable long-range ordering of Mg and Al on the octahedral sublattice (Cameron and Papike 1981). The cation probabilities for this model are given in Appendix 1.2. Peak intensities calculated using the AA model are compared to observed ^{29}Si NMR peak intensities in Figure 6. The Al-O-Al avoidance model is a much better fit to the data than the random model, indicating that Al-O-Al avoidance is operating across most of the solid solution. There are two regions across the solid solution where the model deviates significantly

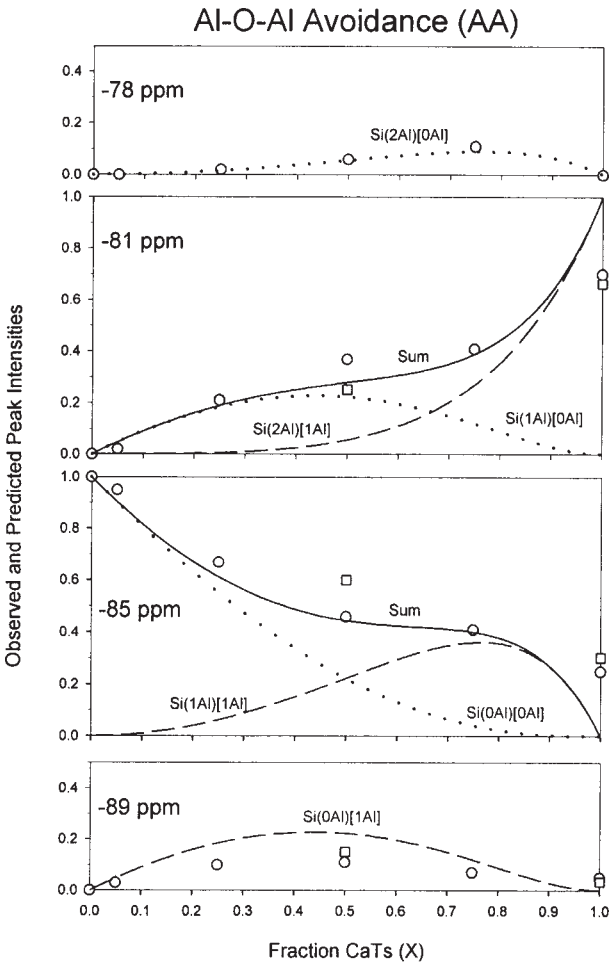

FIGURE 6. Comparison of observed ^{29}Si MAS NMR peak intensities across the diopside-CaTs solid solution with site populations predicted using the Aluminum Avoidance model (AA). The four NMR peaks, near –78 ppm, –81 ppm, –85 ppm, –89 ppm, are shown in **upper** to **lower** boxes, respectively. See Figure 5 for explanation of symbols. The AA model gives an improved fit over the RD model.

from the data: Near 50% CaTs and for compositions >75% CaTs. These two regions will be treated separately.

The poorest fit between Al-O-Al avoidance model and the observed data is at high $^{[4]}$Al concentration, nearing the CaTs end-member (>75% CaTs). The Al-O-Al avoidance model fails as the tetrahedral Al/Si ratio approaches Al/Si = 1, because complete Si-Al ordering is imposed by the Al-O-Al avoidance model in order to avoid Al-O-Al linkages (i.e., the entire chain is ordered into alternating Al-O-Si-O-Al-O-Si…), while the CaTs sample clearly is not fully ordered. Although CaTs has retained 70% order, it clearly also contains Al-O-Al linkages. Circone et al. (1991) observed in mica that, "The probability of Al occupying a site next to Al increases non-linearly with increasing $^{[4]}$Al content." Clearly, the number of Al-O-Al linkages increases from essentially zero at 75% CaTs to a maximum of 0.175 Al-O-Al linkages pfu in end-member CaTs. The number of Al-O-Al linkages in intermediate members of the solid solution could not be measured directly from the observed ^{29}Si MAS NMR peak intensities due to peak overlap. Furthermore, the number of Al-O-Al linkages could not be calculated using the present model, which assumes that the number of Al-O-Al linkages is zero. To determine the number of Al-O-Al linkages, the model must include an estimate the extent of Al-O-Al avoidance via the reaction: Si-O-Si + Al-O-Al = 2 Si-O-Al.

Al-O-Al avoidance with octahedral coupling

The poor fit of the Al-O-Al avoidance model to the ^{29}Si MAS NMR data for compositions near 50% CaTs involves an overestimation of the peak intensity at –89 ppm and the equivalent underestimation of peak intensity at –81 ppm. The discrepancy at –89 ppm indicates that there are fewer Si(0Al)[1Al] environments than would be expected as a random population of Mg and Al on the octahedral site, while at –81 ppm there appear to be more Si(1Al)[0Al] environments than predicted by a random population on the octahedral site. This correlation suggests an association between the tetrahedral and octahedral sublattices, where $^{[4]}$Si-O-$^{[6]}$Mg and $^{[4]}$Al-O-$^{[6]}$Al configurations are preferred relative to the alternate configurations ($^{[4]}$Si-O-$^{[6]}$Al and $^{[4]}$Al-O-$^{[6]}$Mg). This is logical because $^{[4]}$Si-O-$^{[6]}$Mg and $^{[4]}$Al-O-$^{[6]}$Al configurations would provide local charge balance around O atoms. The AAOC model is similar to the AA model above, but also restricts the octahedral cation distribution to the couples $^{[4]}$Si-O-$^{[6]}$Mg and $^{[4]}$Al-O-$^{[6]}$Al. The population of these couples varies as a function of tetrahedral Al/Si ratio, as explained in Appendix 1.3. Peak intensities calculated using the AAOC model are compared to observed ^{29}Si NMR peak intensities in Figure 7. The fit to the peak intensity at –89 ppm for Si(0Al)[1Al] is greatly improved across the solid solution. The fit to the peak intensity at –81 ppm is greatly improved near ~50% CaTs component. This suggests that Mg-Al ordering in M1 is locally coupled to Si-Al ordering on the tetrahedral chain. This coupling would likely be occurring between the M1 and T sites sharing the underbonded O2, where local charge balance is likely to be an important consideration. The possibility of coupling between octahedral and tetrahedral cation ordering, as suggested by our AAOC model, is supported by Monte Carlo simulations (Bosenick et al. 2001), but has not been observed directly in Tschermak pyroxenes.

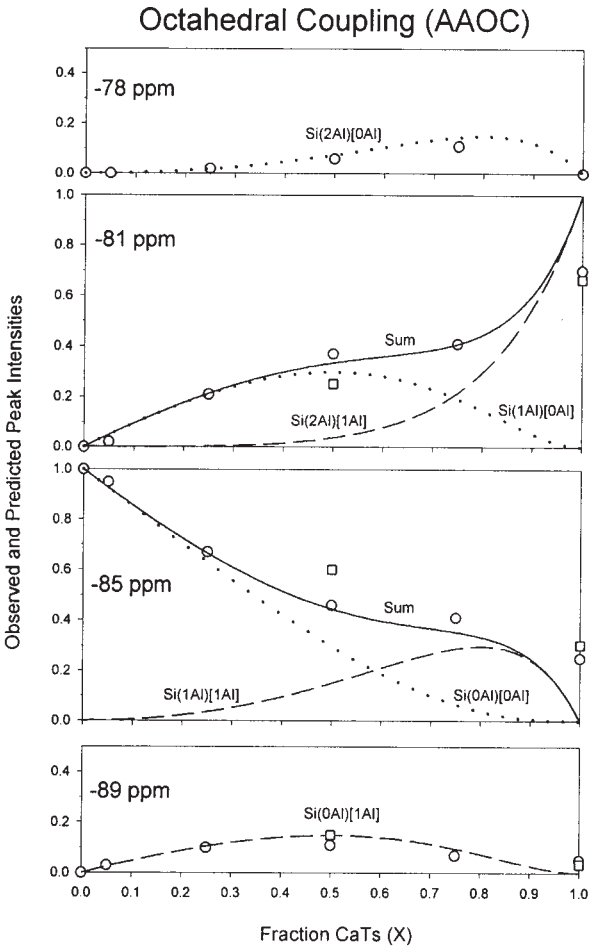

FIGURE 7. Comparison of observed ^{29}Si MAS NMR peak intensities across the diopside-CaTs solid solution with site populations predicted using the model of Aluminum Avoidance with Octahedral Coupling (AAOC). The four NMR peaks, near –78 ppm, –81 ppm, –85 ppm, –89 ppm, are shown in **upper** to **lower** boxes, respectively. See Figure 5 for explanation of symbols. The AAOC model gives the closest fit to the observed NMR data.

Ordering on the octahedral sites is well known in omphacitic pyroxenes, near the midpoint of the solid solution ($Di_{50}Jd_{50}$), where Mg and Al become long-range ordered onto M1 and M11 sites respectively, thus lowering the space group symmetry from *C*2/*c* to *P*2/*n* (see Rossi 1988). In omphacite, it is believed that Mg-Al ordering on M1 is coupled to Ca-Na ordering on M2 to provide local charge balance (Fleet et al. 1978; Davidson and Burton 1987). Our AAOC model suggests a similar association in Tschermak pyroxenes. This would be a short-range phenomenon, however, as long-range ordering between Mg and Al on the octahedral sublattice has not been found previously for intermediate diopside-CaTs pyroxenes. A short-range order model associating $^{[4]}$Al-O-$^{[6]}$Al linkages was suggested by Wood (1976). An ^{27}Al 3QMAS NMR study is underway to examine Mg-Al ordering on the octahedral sublattice and its suspected coupling to tetrahedral Si-Al ordering.

Summary of Si-Al ordering in Ca-Tschermak pyroxenes

Cation distributions predicted by the two Al-O-Al avoidance models presented above (AA and AAOC) give reasonable approximations to the ^{29}Si MAS NMR data to at least 75% CaTs, indicating that Löwenstein's (1954) Al-O-Al avoidance principle is obeyed within the compositional range of natural pyroxenes. Natural pyroxenes typically have <2 mol% CaTs (Dawson and Carswell 1990) but those of eclogites can have as much as 25 mol% CaTs (Dawson and Carswell 1990), or even 50 mol% CaTs in Si-poor rocks (Peacor 1967).

Clearly, neither the AA model nor the AAOC model can predict the observed cation distribution from ^{29}Si MAS NMR data for compositions >75% CaTs (approaching Al/Si = 1), indicating that Löwenstein's (1954) principle is not obeyed for highly aluminous pyroxenes. Deviation from Al-O-Al avoidance is expected to be a maximum for end-member CaTs, which exhibits 0.175 Al-O-Al linkages pfu, as calculated directly from ^{29}Si MAS NMR peak intensities.

The region >75% CaTs in the Di-CaTs solid solution provides a useful test for the limit of utility of the cation-ordering models. Both the AA and AAOC models fail to predict the observed cation ordering for compositions above ~75% CaTs, because these simple statistical models do not account for Al-O-Al formation. To predict the cation distribution in this region, a more sophisticated statistical-thermodynamic model must be applied to the present ^{29}Si MAS NMR data. Several statistical-thermodynamic models are being developed to elucidate Si, Al ordering in aluminosilicates. These models minimize the energy of the "Al-O-Al avoidance" reaction Si-O-Si + Al-O-Al = 2 Si-O-Al, using ^{29}Si MAS NMR spectra to constrain site populations. Potentially useful models include the Homogeneous Distribution of Charge (HDC) model developed for sheet silicates (Herrero et al. 1985; Circone et al. 1991; Welch et al. 1995; Vinograd 1995), the quasi-chemical approximation of Lee and Stebbins (1999) developed for fully polymerized glasses, Monte Carlo methods developed for framework silicates (Dove and Heine 1996; Myers et al. 1998) and the Cluster Variation Method (CVM) developed for sheet silicates (Herrero and Sanz 1991; Vinograd and Putnis 1998), but expanded for ring, and framework aluminosilicates (Vinograd and Putnis 1999). Monte Carlo simulation has very recently been applied to pyroxenes (Bosenick et al. 2001; Warren et al. 2001), but the other methods above would require adaption for use with single chain silicates.

A high degree of short-range order is observed in aluminous Ca-Tschermak pyroxenes, as a result of Al-O-Al avoidance on the tetrahedral sublattice, as suggested by the AA model, possibly combined with coupling between tetrahedral and octahedral cation positions, as suggested by the AAOC model. This implies that Ca-Tschermak pyroxenes have significantly lower configurational entropy than expected from the disordered cation distribution typically associated with space group *C*2/*c*. This has implications for mineral equilibria in lherzolites and eclogites as it will affect the accuracy of thermobarometers (e.g., Brey et al. 1986; Mukhopadhyay 1991; Nimis 1995; Putirka et al. 1996; Nimis and Ulmer 1998), and thermodynamic models involving CaTs pyroxene (Wood 1976; Newton 1977; Wood and Holloway 1984; Haselton et al. 1984; Cohen 1986b; Sack and Ghiorso 1994a, 1994b; Powell and Holland 1999).

ACKNOWLEDGMENTS

This work was funded by NSERC grants to R.W.L. and an Izaak Walton Killam Memorial Postdoctoral Fellowship to R.L.F. We thank the Department of Chemistry at University of Alberta for generous use of their AM-300R spectrometer and the technical assistance of G. Bigam. We also thank D. Caird for technical assistance with the X-ray diffractometer, L. Shi for technical assistance on the EPMA, D. Resultay and M. Labbe for assistance preparing probe mounts, and J.J. Millard for assistance with figures. This work benefited from useful discussions with R.C. Peterson, H.E. Jamieson, and A.A. Poustovetov, and careful reading and thoughtful comments from M.E. Fleet and B.L. Sherriff. We also thank B.L. Phillips, M.D. Welch, and an anonymous reviewer for their helpful comments.

REFERENCES CITED

Armbruster, T. (1999) Si, Al ordering in the double-ring silicate armenite, $BaCa_2Al_6Si_9O_{30}\cdot 2H_2O$: A single-crystal X-ray and ^{29}Si MAS NMR study. American Mineralogist, 84, 92–101.

Benna, P., Tribaudino, M., and Bruno, E. (1988) Crystal structure of $Di_{50}CaTs_{50}$ synthetic clinopyroxene ($CaMg_{0.5}AlSi_{1.5}O_6$). Crystal chemistry along the Di-CaTs join. Mineralogy and Petrology, 38, 189–200.

Bosenick, A., Dove, M.T., Myers, E.R., Palin, E.J., Sainz-Diaz, C.I., Guiton, B.S., Warren, M.C., Craig, M.S., and Redfern, S.A.T. (2001) Computational methods for the study of energies of cation distributions: applications to cation-ordering phase transitions and solid solutions. Mineralogical Magazine, 65, 193–219.

Brey, G.P., Nickel, K.G., and Kogarko, L. (1986) Garnet-pyroxene equilibria in the system CaO-MgO-Al_2O_3-SiO_2 (CMAS): prospects for simplified ('T-independent') lherzolite barometry and an eclogite-barometer. Contributions to Mineralogy and Petrology, 92, 448–455.

Cameron, M. and Papike, J.J. (1981) Structural and chemical variations in pyroxenes. American Mineralogist, 66, 1–50.

Carswell, D.A. (1991) The garnet-orthopyroxene Al barometer: problematic application to natural garnet lherzolite assemblages. Mineralogical Magazine, 55, 19–31.

Cheng, X., Zhao, P., and Stebbins, J.F. (2000) Solid state NMR study of oxygen site exchange and Al-O-Al site concentration in analcime. American Mineralogist, 85, 1030–1037.

Circone, S., Navrotsky, A., Kirkpatrick, R.J., and Graham, C. M. (1991) Substitution of $^{[6,4]}$Al in phlogopite: Mica characterization, unit-cell variation, ^{27}Al and ^{29}Si MAS-NMR spectroscopy, and Al-Si distribution in the tetrahedral sheet. American Mineralogist, 76, 1485–1501.

Cohen, R.E. (1985) Thermodynamics of Aluminous Pyroxenes: Effects of Short-Range Order. PhD Thesis, Harvard University, Cambridge, MS. April 1985.

———(1986a) Statistical mechanics of coupled solid solutions in the dilute Limit. Physics and Chemistry of Minerals, 13, 174–182.

———(1986b) Configurational thermodynamics of aluminous pyroxenes: A generalized pair approximation. Physics and Chemistry of Minerals, 13, 183–197.

Cohen, R.E. and Burnham, C.W. (1985) Energetics of ordering in aluminous pyroxenes. American Mineralogist, 70, 559–567.

Davidson, P.M. and Burton, B.P. (1987) Order-disorder in omphacitic pyroxenes: A model for coupled substitution in the point approximation. American Mineralogist, 72, 337–344.

Dawson, J.B. and Carswell, D.A. (1990) High temperature and ultra-high pressure eclogites. In D.A. Carswell, Ed., Eclogite Facies Rocks, 314–349 p. Chapman and Hall, New York.

Dove, M.T. and Heine, V. (1996) The use of Monte Carlo methods to determine the distribution of Al and Si cations in framework aluminosilicates from ^{29}Si MAS NMR data. American Mineralogist, 81, 39–44.

Engelhardt, G. and Michel, D. (1987) High-Resolution Solid-State NMR of Silicates and Zeolites. 485 p. John Wiley & Sons, Ltd. New York.

Fleet, M.E., Herzberg, C.T., Bancroft, G.M., and Aldridge, L.P. (1978) Omphacite studies, I: The $P2/n \rightarrow C2/c$ transformation. American Mineralogist, 63, 1100–1106.

Fyfe, C.A. (1983) Solid State NMR for Chemists. 593p. C.F.C. Press, Guelph, Ontario.

Ganguly, J. and Ghose, S. (1979) Aluminous orthopyroxene: Order-disorder, thermodynamic properties, and petrologic implications. Contributions to Mineralogy and Petrology, 69, 375–385.

Gasparik, T. (1981) Mixing properties of the binary Jd-CaTs. EOS Transactions of the American Geophysical Union, 62, 412.

Haselton, H.T. Jr., Hemingway, B.S., and Robie, R.A. (1984) Low-temperature heat capacities of $CaAl_2SiO_6$ glass and pyroxene and thermal expansion of $CaAl_2SiO_6$ pyroxene. American Mineralogist, 69, 481–489.

Hays, J.F. (1966) Lime-alumina-silica. Carnegie Institute of Washington Yearbook,

65, 234–239.
Herrero, C.P. and Sanz, J. (1991) Short-range order of the Si, Al distribution in layer silicates. Journal of Physics and Chemistry of Solids, 52, 1129–1135.
Herrero, C.P., Sanz, J., and Serratosa, J.M. (1985) Si, Al distribution in micas: analysis by high-resolution ^{29}Si NMR spectroscopy. Journal of Physics C: Solid State Physics, 18, 13–22.
Kato, M. and Hattori, T. (1998) Ordered distribution of aluminum atoms in analcime. Physics and Chemistry of Minerals, 25, 556–565.
Kirkpatrick, R.J. (1988) MAS NMR spectroscopy of minerals and glasses. In F.C. Hawthorne, Ed., Spectroscopic Methods in Mineralogy and Geology, p. 341–403. Reviews in Mineralogy, MineralogicalSociety of America, Washington, D.C.
Kirkpatrick, R.J., Smith, K.A., Schramm, S., Turner, G., and Yang, W.-H. (1985) Solid-state nuclear magnetic resonance spectroscopy of minerals. Annual Review of Earth and Planetary Sciences, 13, 29–47.
Kirkpatrick, R.J., Oestrike, R., Weiss, C.A. Jr., Smith, K.A., and Oldfield, E. (1986) High- resolution ^{27}Al and ^{29}Si NMR spectroscopy of glasses and crystals along the join $CaMgSi_2O_6$-$CaAl_2SiO_6$. American Mineralogist, 71, 705–711.
Kushiro, I. (1976) Changes in viscosity and structure of melt of $NaAlSi_2O_6$ composition at high pressures. Journal of Geophysical Research, 81, 6347–6350.
Lausen, S.K., Lindgreen, H., Jakobsen, H.J., and Nielsen, N.C. (1999) Solid-state ^{29}Si MAS NMR studies of illite and illite-smectite from shale. American Mineralogist, 84, 1433–1438.
Lee, S.K. and Stebbins, J.F. (1999) The degree of aluminum avoidance in aluminosilicates glasses. American Mineralogist, 84, 937–945.
Lippmaa, E., Mägi, M., Samoson, A., Engelhardt, G., and Grimmer, A.-R. (1980) Structural studies of silicates by solid-state high-resolution ^{29}Si NMR. Journal of the American Chemical Society, 102, 4889–4893.
Löwenstein, W. (1954) The distribution of aluminum in the tetrahedra of silicates and aluminates. American Mineralogist, 39, 92–96.
Mukhopadhyay, B. (1991) Garnet-clinopyroxene geobarometry: The problems, a prospect, and an approximate solution with some applications. American Mineralogist, 76, 512–529.
Myers, E.R., Heine, V., and Dove, M.T. (1998) Thermodynamics of Al/Al avoidance in the ordering of Al/Si tetrahedral framework structures. Physics and Chemistry of Minerals, 25, 457–464.
Newton, R.C. (1977) Thermochemistry of garnets and aluminous pyroxenes in the CMAS system. In D.G. Fraser, Ed., Thermodynamics in Geology, p. 29–55. D. Reidel Publishing Company, Holland.
Nimis, P. (1995) A clinopyroxene geobarometer for basaltic systems based on crystal-structure modeling. Contributions to Mineralogy and Petrology, 121, 115–125.
Nimis, P. (1999) Clinopyroxene geobarometry of magmatic rocks. Part 2. Structural geobarometers for basic to acid, tholeiitic and mildly alkaline magmatic systems. Contributions to Mineralogy and Petrology, 135, 62–74.
Nimis, P. and Ulmer, P. (1998) Clinopyroxene geobarometry of magmatic rocks. Part 1. An expanded structural geobarometer for anhydrous and hydrous, basic and ultrabasic systems. Contributions to Mineralogy and Petrology, 133, 122–135.
Okamura, F.P., Ghose, S., and Ohashi, H. (1974) Structure and crystal chemistry of calcium Tschermak's pyroxene, $CaAlAlSiO_6$. American Mineralogist, 59, 549–557.
Peacor, D.R. (1967) Refinement of the crystal structure of a pyroxene of formula $M_I M_{II} (Si_{1.5}Al0_{0.5})O_6$. American Mineralogist, 52, 31–41.
Phillips, B.L., Kirkpatrick, R.J., and Carpenter, M.A. (1992) Investigation of short-range Al, Si order in synthetic anorthite by ^{29}Si MAS NMR spectroscopy. American Mineralogist, 77, 484–494.
Phillips, B.L., McGuinn, M.D., and Redfern, S.A.T. (1997) Si-Al order and the $\bar{I}1$–$I2/c$ structural phase transition in synthetic $CaAl_2Si_2O_8$-$SrAl_2Si_2O_8$ feldspar: A ^{29}Si MAS-NMR spectroscopic study. American Mineralogist, 82, 1–7.
Phillips, B.L., Xu, H., Heaney, P.J., and Navrotsky, A. (2000) ^{29}Si and ^{27}Al MAS NMR spectroscopy of β-eucryptite ($LiAlSiO_4$): The enthalpy of Si,Al ordering. American Mineralogist, 85, 181–188.
Powell, R. and Holland, T. (1999) Relating formulations of the thermodynamics of mineral solid solutions: Activity modeling of pyroxenes, amphiboles, and micas. American Mineralogist, 84, 1–14.
Putirka, K., Johnson, M., Kinzler, R., Longhi, J., and Walker, D. (1996) Thermobarometry of mafic igneous rocks based on clinopyroxene-liquid equilibria, 0–30 kbar. Contributions to Mineralogy and Petrology, 123, 92–108.
Putnis, A. and Angel, R.J. (1985) Al, Si ordering in cordierite using 'Magic Angle Spinning' NMR. II: Models of Al, Si order from NMR data. Physics and Chemistry of Minerals, 12, 217–222.
Rossi, G. (1988) A review of the crystal-chemistry of clinopyroxenes in eclogites and other high-pressure rocks. In D.C. Smith, Ed., Eclogites and Eclogite-facies Rocks. Developments in Petrology, 12, 237–270.
Sack, R.O. and Ghiorso, M.S. (1994a) Thermodynamics of multicomponent pyroxenes: I. Formulation of a general model. Contributions to Mineralogy and Petrology, 116, 277–286.
Sack, R.O. and Ghiorso, M.S. (1994b) Thermodynamics of multicomponent pyroxenes: II. Phase relations in the quadrilateral. Contributions to Mineralogy and Petrology, 116, 287–300.
Sanz, J. and Serratosa, J.M. (1984) ^{29}Si and ^{27}Al high-resolution MAS-NMR spectra of phyllosilicates. Journal of the American Chemical Society, 106, 4790–4793.
Sherriff, B.L., Grundy, H.D., and Hartman, J.S. (1991) The relationship between ^{29}Si MAS NMR chemical shift and silicate mineral structure. European Journal of Mineralogy, 3, 751–768.
Sherriff, B.L., Sokolova, E.V., Kabalov, Y.K., Teertstra, D.K., Kunath-Fandrei, G., Goetz, S., and Jager, C. (1998) Intermediate scapolite: ^{29}Si MAS and ^{27}Al SATRES NMR spectroscopy and Rietveld structure-refinement. Canadian Mineralogist, 36, 1267–1283.
Sherriff, B.L., Jenkins, D.M., Kunath-Fandrei, G., and Goetz, S. (1999) ^{23}Na,^{29}Si, and ^{71}Ga MAS-NMR spectroscopy of synthetic gallian-fluor-amphiboles. American Mineralogist, 84, 1033–1040.
Taylor, W.R. (1998) An experimental test of some geothermometer and geobarometer formulations for upper mantle peridotites with application to the thermobarometry of fertile lherzolite and garnet websterite. Neues Jahrbuch für Mineralogie, Abhandlungen, 172, 381–408.
Tossell, J.A. (1993) A theoretical study of the molecular basis of the Al avoidance rule and of the spectral characteristics of Al-O-Al linkages. American Mineralogist, 78, 911–920.
Vinograd, V.L. (1995) Substitution of $^{[4]}$Al in layer silicates: Calculation of the Al-Si configurational entropy according to ^{29}Si NMR spectra. Physics and Chemistry of Minerals, 22, 87–98.
Vinograd, V.L. and Putnis, A. (1998) Calculation of the configurational entropy of Al, Si in layer silicates using the cluster variation method. Physics and Chemistry of Minerals, 26, 135–148.
Vinograd, V.L. and Putnis, A. (1999) The description of Al, Si ordering in aluminosilicates using the cluster variation method. American Mineralogist, 84, 311–324.
Warren, M.C., Dove, M.T., Myers, E.R., Bosenick, A., and Palin, E.J. (2001) Monte Carlo methods for the cation ordering in minerals. Mineralogical Magazine, 65, 221–248.
Welch, M.D., Barras, J., and Klinowski, J. (1995) A multinuclear NMR study of clinochlore. American Mineralogist, 80, 441–447.
Welch, M.D., Liu, S., and Klinowski, J. (1998) ^{29}Si MAS NMR systematics of calcic and sodic-calcic amphiboles. American Mineralogist, 83, 85–96.
Wood, B.J. (1976) Mixing properties of tschermakitic clinopyroxenes. American Mineralogist, 61, 599–602.
Wood, B.J. and Holloway, J.R. (1984) A thermodynamic model for subsolidus equilibria in the system CaO-MgO-Al_2O_3-SiO_2. Geochimica et Cosmochimica Acta, 48, 159–176.
Yoshino, T., Yamamoto, H., Okudaira, T., and Torium, M. (1998) Crustal thickening of the lower crust of the Kohistan arc (N. Pakistan) deduced from Al zoning in clinopyroxene and plagioclase. Journal of Metamorphic Geology, 16, 729–748.

MANUSCRIPT RECEIVED OCTOBER 5, 2000
MANUSCRIPT ACCEPTED AUGUST 20, 2001
MANUSCRIPT HANDLED BY BRIAN PHILLIPS

APPENDIX 1: ORDERING MODELS EXPLAINED AS CONSISTENT WITH THE HERRERO ET AL. (1985) MODEL

Random distribution model (RD)

If p and q are the mole fractions of tetrahedral Si and Al respectively, the calculated probabilities for the three possible tetrahedral environments around Si [i.e., Si(0Al) (or Si-O-Si-O-Si), Si(1Al) (or Si-O-Si-O-Al), and Si(2Al) (or Al-O-Si-O-Al)] are, respectively, p^2, $2pq$, and q^2. This represents a statistical binomial distribution with no restriction on occupancy of neighboring tetrahedra.

Now p and q can be converted into terms relevant to the chemical formula of the pyroxene, $Ca[Mg_{1-x}Al_x](Si_{1-x/2}Al_{x/2})_2O_6$. Here $p = 1 - x/2$ and $q = x/2$, where x is the fraction of $CaAl_2SiO_6$ or CaTs component in the solid solution. This gives a statistical binomial distribution of $(1 - x/2)^2$, $2(1 - x/2)(x/2)$, $(x/2)^2$, as shown in Appendix Table 1. Because NMR peak intensities are also affected by octahedral cation substitution, the cation population expressions have been extended to include a ran-

APPENDIX TABLE 1. Probability of cation populations around Si for a random distribution of cations (Model 1: RD)

Tetrahedral NN Cations (same chain)		Octahedral NN Cation (1 site model)	
		Mg (1–x)	Al (x)
Si (1–x/2)	Si (1–x/2)	(1–x/2)^2·(1–x)	(1–x/2)^2·x
Si (1–x/2)	Al (x/2)	2·(1–x/2)·(x/2)·(1–x)	2·(1–x/2)·(x/2)·x
Al (x/2)	Al (x/2)	(x/2)^2·(1–x)	(x/2)^2·x

Notes: x = mole fraction CaTs component ($CaAl_2SiO_6$). Fractional contents of $^{[4]}$Al, Si, $^{[6]}$Al, and Mg are indicated in brackets below element.

dom distribution of cations at the octahedral site (Al = x, Mg = 1 – x), as shown in Appendix Table 1.

Al-O-Al avoidance model (AA)

In this model, no two Al cations can be adjacent to one another on the tetrahedral chain (i.e., Al-O-Al are not allowed). This restriction leaves only two possible associations between corner-sharing tetrahedra. These are Si-O-Al and Si-O-Si. Thus, if p and q are the fractional contents of tetrahedral Si and Al, respectively, the probability of occurrence of Si-O-Al is 2q (similar to random model except the probability of Si as neighbor to Al equals 1 as Al-O-Al is not allowed). It follows that the probability of occurrence of Si-O-Si will be 1–2q. If now we restrict our analysis to cases where the first tetrahedral site in the pair contains Si, the probability occurrence of Si-O-Al becomes q. Normalized probabilities for Si-O-Al and Si-O-Si will be (Herrero et al. 1985):

$$P_{Si\text{-}O\text{-}Al} = q/[q + (1 - 2q)] = q/p = a \quad (1)$$

$$P_{Si\text{-}O\text{-}Si} = (1 - 2q)/p = 1 - q/p = s \quad (2)$$

The probabilities of the three probable environments around Si in pyroxene follow the binomial distribution a^2, 2as, s^2.

This binomial distribution can also be converted into terms relevant to the diopside-CaTs pyroxene solid solution. Because $a = P_{Si\text{-}O\text{-}Al} = q/p$, the probability of occurrence of Al next to Si is a function of the tetrahedral Al/Si ratio in pyroxene, where a = Al/Si and s = 1 – Al/Si. The binomial distribution for Al-O-Al avoidance becomes (Al/Si)^2, 2(Al/Si)(1 – Al/Si), (1 – Al/Si)^2 as shown in Appendix Table 2. Cation population expressions have been extended to include a random distribution of cations at the octahedral site (Al = x, Mg = 1 – x, where x is mol fraction CaTs component), as shown in Appendix Table 2.

Al-O-Al avoidance with octahedral coupling (AAOC):

This model treats the tetrahedral cation distribution as in model 2 above, as shown in Appendix Table 3. In addition, however, the octahedral cation distribution is treated as non-random. This model applies tetrahedral-octahedral cation coupling, where $^{[4]}$Si-O-$^{[6]}$Mg and $^{[4]}$Al-O-$^{[6]}$Al couples are preferred. In this model, all available $^{[6]}$Mg (= 1 – x) is coupled to $^{[4]}$Si. Thus the fraction of $^{[4]}$Si-O-$^{[6]}$Mg linkages is 1 – x. Remaining Si will form $^{[4]}$Si-O-$^{[6]}$Al linkages. The number of $^{[4]}$Si-O-$^{[6]}$Al linkages is calculated by subtracting the number of $^{[4]}$Si-O-$^{[6]}$Mg linkages from the total available Si, such as $n_{(^{[4]}Si\text{-}O\text{-}^{[6]}Al)} = Si_{total} - n_{(^{[4]}Si\text{-}O\text{-}^{[6]}Mg)} = (1 - x/2) - (1 - x) = x/2$ (where n is the number of relevant linkages). Normalizing to the sum of both observable populations ($^{[4]}$Si-O-$^{[6]}$Mg + $^{[4]}$Si-O-$^{[6]}$Al = 1 – x + x/2 = 1 – x/2) gives probabilities for the observed linkages as:

$$p_{(^{[4]}Si\text{-}O\text{-}^{[6]}Al)} = (x/2)/(1 - x/2) = Al/Si \quad (3)$$

$$p_{(^{[4]}Si\text{-}O\text{-}^{[6]}Mg)} = 1 - Al/Si \quad (4)$$

where Al/Si represents the ratio of $^{[4]}$Al to Si at the tetrahedral site. The above populations are used for the octahedral Al and Mg cations, respectively, as shown in Appendix Table 3.

APPENDIX TABLE 2. Probability of cation populations around Si assuming complete Al-O-Al avoidance (Herrero et al. 1985) on tetrahedral site (and random distribution of Al on M1) (Model 2: AA)

Tetrahedral NN Cations (same chain)		Octahedral NN Cation (1 site model)	
		Mg (1–x)	Al (x)
Si (1–Al/Si)	Si (1–Al/Si)	(1–Al/Si)^2·(1–x)	(1–Al/Si)^2·x
Si (1–Al/Si)	Al (Al/Si)	2·(1–Al/Si)·(Al/Si)·(1–x)	2·(1–Al/Si)·(Al/Si)·x
Al (Al/Si)	Al (Al/Si)	(Al/Si)^2·(1–x)	(Al/Si)^2·x

Notes: x = mole fraction CaTs component ($CaAl_2SiO_6$). Al/Si refers to ratio of $^{[4]}$Al to Si.

APPENDIX TABLE 3. Probability of cation populations around Si assuming Al-O-Al avoidance on tetrahedral site, and with non-random distribution of cations on M1 (i.e., $^{[4]}$Si-O-$^{[6]}$Mg and $^{[4]}$Al-O-$^{[6]}$Al preferred) (Model 3: AAOC)

Tetrahedral NN Cations (same chain)		Octahedral NN Cation (1 site model)	
		Mg (1–Al/Si)	Al (Al/Si)
Si (1–Al/Si)	Si (1–Al/Si)	(1–Al/Si)^3	(1–Al/Si)^2·(Al/Si)
Si (1–Al/Si)	Al (Al/Si)	2·(1–Al/Si)^2·(Al/Si)	2·(1–Al/Si)·(Al/Si)^2
Al (Al/Si)	Al (Al/Si)	(Al/Si)^2·(1–Al/Si)	(Al/Si)^3

Notes: Al/Si refers to ratio of $^{[4]}$Al to Si.